Research article

Magnetic modulation in mechanical alloyed $Cr_{1.4}Fe_{0.6}O_3$ oxide

RN Bhowmik*, M Nrisimha Murty and E Sekhar Srinadhu

Address: Department of Physics, Pondicherry University, R. Venkataraman Nagar, Kalapet, Pondicherry-605014, India

Email: RN Bhowmik* - rnbhowmik.phy@pondiuni.edu.in; M Nrisimha Murty - murtydattu27@gmail.com; E Sekhar Srinadhu - sekharsrinadhu@gmail.com

* Corresponding author

Abstract

The compound $Cr_{1.4}Fe_{0.6}O_3$ has been synthesized through mechanical alloying of Cr_2O_3 and α-Fe_2O_3 powders and subsequent thermal annealing. The XRD spectrum, SEM picture and microanalysis of EDAX spectrum have been used to understand the structural evolution during alloy formation. The alloyed samples have been matched to rhombohedral structure with R3C space group. The observation of a modulated magnetic order confirmed the systematic diffusion of Fe atoms into the Cr sites of lattice structure. A field induced magnetic behaviour has been noted in the field dependence of magnetization data of the annealed samples. This feature is significantly different from that of the mechanical alloyed samples. The experimental results also provided the indications of considering the present material as a potential candidate for opto-electronic applications.

PACS Codes: 75.30.-m, 75.20.En, 81.40.Rs

1. Introduction

In recent years extensive research efforts have been given to the formation of new magnetic oxides, considering their potential applications in the field of micro-electronics and multifunctional devices [1,2]. In order to search for the new class of materials, it has been found that solid solution of mixed metal oxides might be a potential candidate, having advantage of easy alloying due to ionic radius of same order [3,4]. $Fe_{2-x}Cr_xO_3$ is one such compound series, which can be formed through the alloying of α-Fe_2O_3 and Cr_2O_3 oxides [5,6]. The interesting points are that both α-Fe_2O_3 and Cr_2O_3 stabilized into rhombohedral crystal structure with space group R3C [4,7] and both are antiferromagnetic insulator [8]. Cr_2O_3 oxide is a well known compound for the prediction and experimental observation of large magneto-electric (ME) effect [9,10]. The ME effect is generally small in symmetric non-magnetic insulators [11]. The low magnetic moment

and low antiferromagnetic ordering temperature (T_N) of single phase Cr_2O_3 (~310 K) is also not suitable for obtaining large magneto-electric effect, as well as for applications [12,13]. Recently, the exhibition of large magnet-electric effect in Cr_2O_3 was attributed [14] to a possible change of magnetic space group symmetry. This triggered the alloying of $Fe_{2-x}Cr_xO_3$ series by mixing a suitable amount of Fe_2O_3 (T_N ~ 950 K) [4,8] in Cr_2O_3 oxide. The study of this series also remained attractive due to its promising applications in the field of opto-electronic materials. The immediate effect is that $Fe_{2-x}Cr_xO_3$ series has shown the enhancement in photo-conductivity with the increase of Cr content [2,15]. In order to understand the modified photo-conductivity, as well as magneto-electric effect, one needs to realize the correlation between crystal structure and magnetic ordering in the compound. The correlation between its crystal structure and magnetism would also be relevant to gain the properties of Cr-Fe interface [2].

In literature, the antiferromagnetic ordering of spins in both α-Fe_2O_3 and Cr_2O_3 has been explained in terms of super exchange interactions (Cr-O-Cr, Fe-O-Fe) [4,8]. Neutron diffraction study explained the drastic variation of T_N (~310 K for Cr_2O_3 and ~950 K for Fe_2O_3) due to a different kind of magnetic structure, although α-Fe_2O_3 and Cr_2O_3 have shown identical crystal structure. Earlier reports [4,7,8] suggested that the spin moments of Cr^{3+} ($3d^3$) ions in Cr_2O_3 are arranged in + - + - (+ $\equiv$ up spin, - $\equiv$ down spin) sequence along the [111] axis, whereas the spins of Fe^{3+} ($3d^5$) ions in α-Fe_2O_3 are ordered in the + - - + sequence. Hence, it is expected that the substitution of Fe^{3+} ($3d^5$) by Cr^{3+} ($3d^3$) in $Fe_{2-x}Cr_xO_3$ solid solution would modify the sequence of spins ordering, as well as the nature of superexchange interactions. Form the phase diagram of $Fe_{2-x}Cr_xO_3$ [4] one could estimate an equal probability of Fe-O-Fe, Fe-O-Cr, Cr-O-Cr superexchange interactions near to x = 1 and no significant change in the ordering of spins. This resulted in a slow variation of T_N with Cr content in the region $0.90 < x \leq 1.52$ [4]. However, the nature of spin ordering may not follow the conventional structure due to the change of magnetic space group symmetry. The modulated (perturbed) local magnetic order could be expected during the diffusion of Fe atoms into Cr sites. To our knowledge, the magnetic ordering of $Fe_{2-x}Cr_xO_3$ compound is not clear till date. Attempts were made to understand the structural and magnetic properties of $Fe_{2-x}Cr_xO_3$ compound by reducing the particle size in nanometer range using various chemical routes [16,17]. However, enough attention was not given in the reported works to realize the effect of modulated spin structure on the properties of $Fe_{2-x}Cr_xO_3$ compound.

In this work, $Cr_{1.4}Fe_{0.6}O_3$ compound has been synthesized using the novel technique of Mechanical alloying [18]. Attempts have been made to investigate the associated structural and magnetic evolution in different states of mechanical alloying and annealing of the samples. The nature of magnetic order, i.e., antiferromagnet or ferromagnet or the mixed properties of ferromagnet and antiferromagnet, was understood for $Cr_{1.4}Fe_{0.6}O_3$ compound.

2. Experimental

2.1. Sample preparation

The stoichiometric amounts of high purity α-Fe_2O_3 and Cr_2O_3 were mixed for the preparation of $Cr_{1.4}Fe_{0.6}O_3$ compound. The initial colours of α-Fe_2O_3 and Cr_2O_3 were red and green, respectively. The mixture of Fe_2O_3 and Cr_2O_3 was ground using agate mortar and pestle for nearly two hours in atmospheric conditions. The ground powder was mechanical alloyed using Fritsch planetary mono mill (pulverisette 7). The material and balls (combination of 10 mm Silicon Nitride and 5 mm Tungsten Carbide) mass ratio was maintained to 1:7. The mechanical alloying was carried out in atmospheric condition up to 84 hours in a silicon nitride (Si_3N_4) bowl with rotational speed 300 rpm. The non-magnetic balls and bowl (Silicon Nitride and Tungsten Carbide) were selected to avoid the magnetic contamination during the milling process. The milling process was intermediately stopped to monitor the uniform alloying of the mixture and to minimize the local heat generation that might occur during continuous milling. A small quantity of alloyed sample after 24 hours and 48 hours was taken out to check the structural phase evolution. The alloyed samples with different milling hours were made into pellets. The pellets of 84 hours milled sample were placed in alumina crucibles and annealed at 700°C in atmospheric conditions. After annealing for 1 hour, 3 hours and 17 hours, individual pellet was directly air quenched to room temperature. The mechanical alloyed samples was denoted as MA**h**, where **h** = 0, 24, 48 and 84 for alloying time 0, 24 hours, 48 hours and 84 hours, respectively. The samples annealed at 700°C were denoted as SN**t**, where **t** = 1, 3 and 17 for annealing time 1 hour, 3 hours and 17 hours, respectively.

2.2. Sample characterization and measurements

The crystalline phase of alloyed and annealed samples was characterized by recording the X-ray Diffraction spectra in the 2θ range 10–90° with step size 0.01°. The Cu-Kα radiation from the X-ray Diffractometer (model: X pert Panalytical) were employed to record the room temperature spectrum of each sample. The scanning electron microscopic (SEM) picture of the samples was taken using HITACHI S-3400N model. Elemental composition of the samples was obtained from the energy dispersive analysis of x-ray (EDX) spectrum. The magnetic properties of the samples were studied by the measurement of magnetization as a function of temperature and magnetic field using vibrating sample magnetometer (Model: Lakeshore 7400). The temperature (300 K–900 K) dependence of magnetization was measured by attaching a high temperature oven to the vibrating sample magnetometer. The temperature dependence of magnetization was carried out at 1 kOe magnetic field by increasing the temperature from 300 K to 900 K (ZFC mode) and reversing back the temperature to 300 K in the presence of same applied field 1 kOe (FC mode). It should be noted that the ZFC mode followed here is slightly different from the conventional zero field cooling (ZFC) measurement, where the sample is first cooled without applying magnetic field from the temperature greater than T_C to the temperature lower than T_C and magnetization measurement in the presence of magnetic field starts with the increase of temperature. The field dependence of magnetization at 300 K was measured within ± 15 kOe.

3. Results and discussion

3.1. Structural properties

Fig. 1 shows the XRD spectrum of mechanical alloyed and subsequent annealed samples. The MA0 sample (before milling) shows a mixed pattern of Fe_2O_3 and Cr_2O_3 phases. The peaks of Fe_2O_3 and Cr_2O_3 phases are well separated before mechanical alloying. As the alloying process continued by increasing the milling time, the individual peaks of Fe_2O_3 and Cr_2O_3 phases are merging to each other. The intensity of peaks is decreasing as the milling time increases up to 84 hours. At the same time broadness and symmetry in the shape of the peaks are increasing. Subsequent annealing of MA84 sample at 700°C, again, increases the peak intensity, along with increasing sharpness, with the increase of annealing time up to 17 hours. The undergoing phase evolution during the mechanical alloying and annealing process is clearly demonstrated in Fig. 2 for (104) and (110) peak positions. In the (MA0) mixed sample, the peaks position of Cr_2O_3 sample are at higher 2θ value with respect to Fe_2O_3 sample. The notable feature is that peaks of Fe_2O_3 sample disappear with the increase of milling time and the XRD pattern of alloyed com
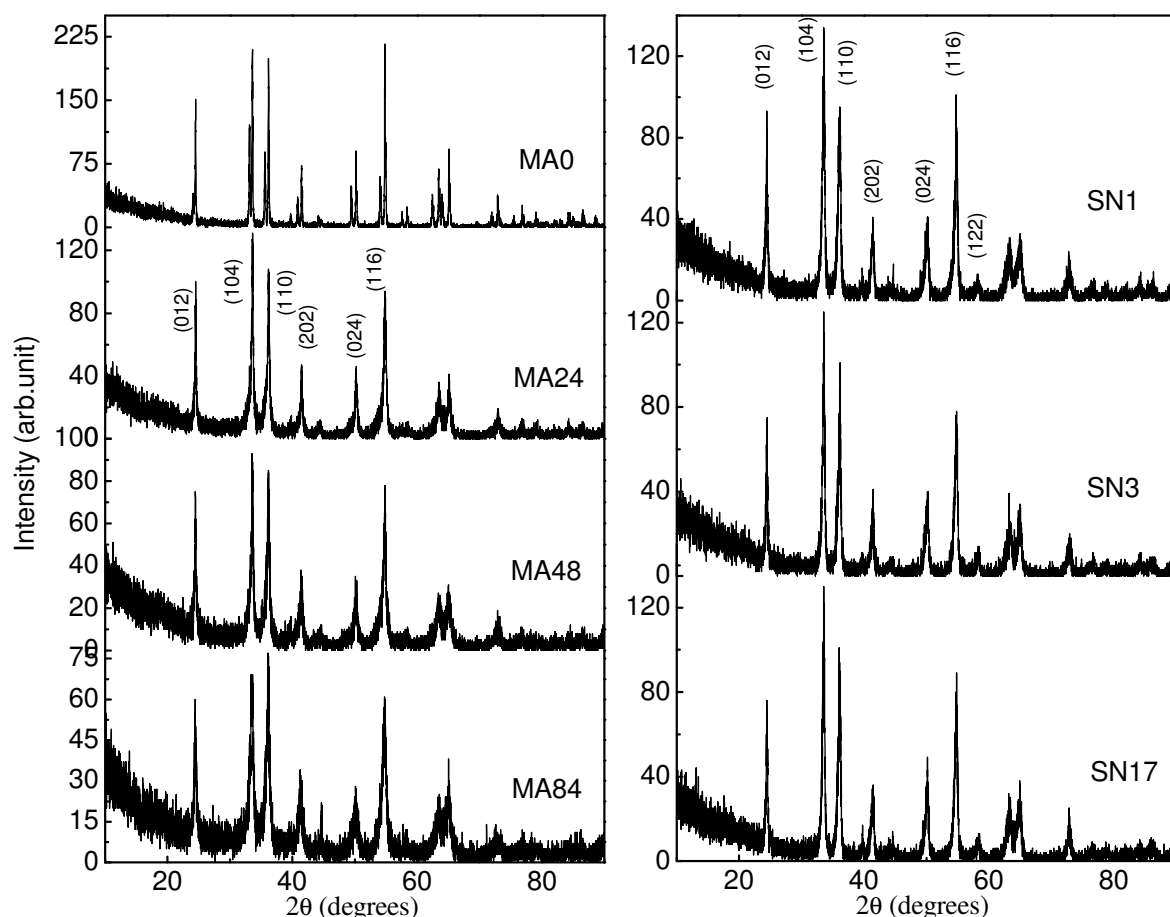
Figure 1
The evolution of XRD spectrum in alloyed sample with milling time and annealing time.
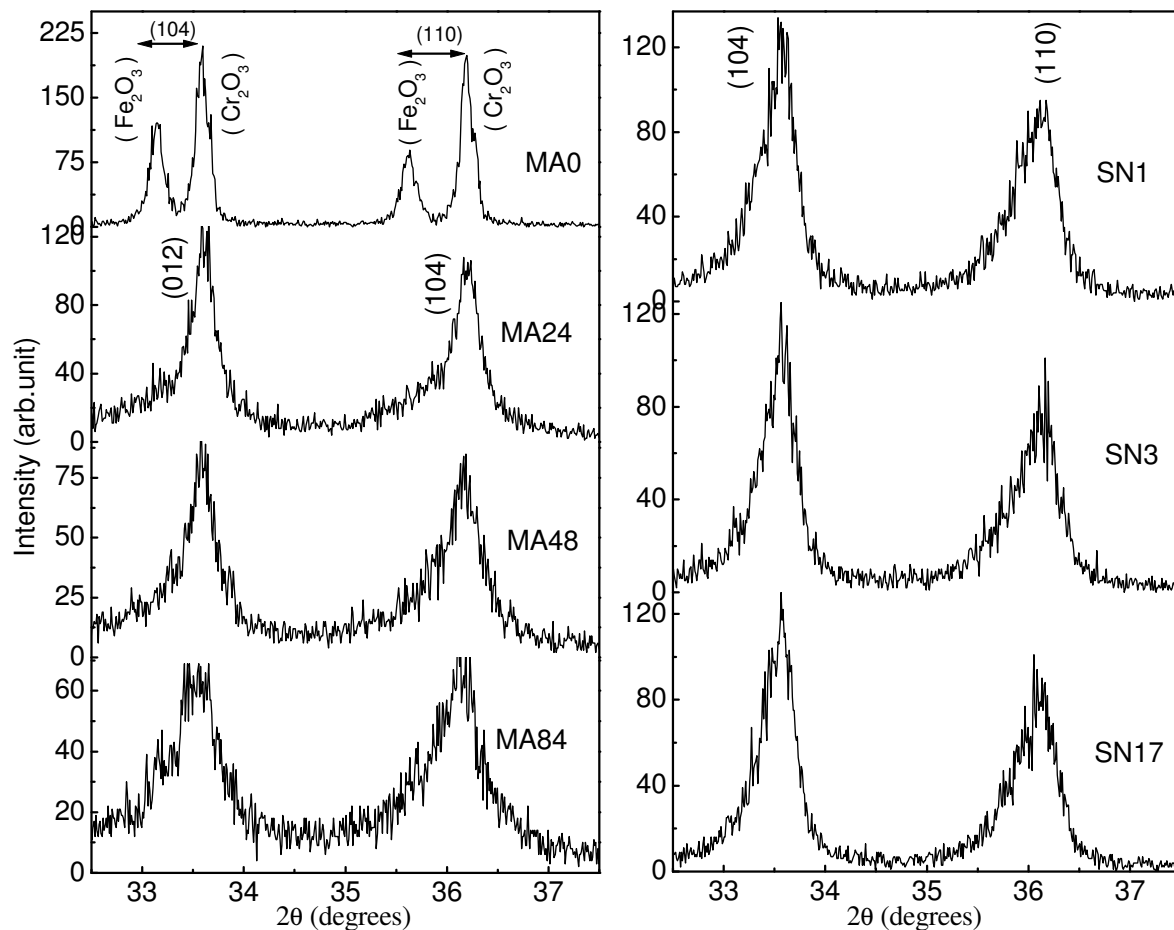
Figure 2
The evolution of spectrum of the alloyed samples for (104) and (110) XRD peaks.

pound is tending to achieve the character of Cr_2O_3. This indicates the diffusion of Fe atoms into the lattice sites of Cr atoms to form a solid solution of $Cr_{1.4}Fe_{0.6}O_3$.

Now, we understand the grain size refinement process. We have determined the grain size of alloyed samples from the prominent (012), (104), (110) and (116) XRD peaks using Debye-Scherrer formula: $\langle d \rangle = \frac{0.089*180*\lambda}{3.14*\beta*\cos\theta_C} nm$, where $2\theta_C$ is the position of peak center, λ is the wavelength of X-ray radiation (1.54056 Å), β is the full width at the half maximum of peak height (in degrees). The $2\theta_C$ and β values were calculated by fitting the XRD peak profile to Lorentzian shape. The average grain size of the alloyed compound is found to be in nanometer range, which suggested the nanocrystalline structure of the material. The grain size of the alloyed compound slowly decreases with the increase of milling time (i.e., <d> ∼ 26 nm for MA24, 22 nm for MA48, and 15 nm for MA84 sample). The thermal annealing of MA84 (lowest grain size) sample at 700°C activates the increase of grain size (i.e., <d> ∼ 19 nm, 21 nm and 22 nm for annealing time

1 hour, 3 hours and 17 hours, respectively). However, a finite amount of instrumental broadening and lattice strain may affect the XRD peak broadening in mechanical alloyed samples and hence, the grain size estimation based on the Debye-Scherrer formula may be far from good accuracy. To check these two factors, Williamson-Hall plot [19] was used. The Williamson-Hall equation is $\beta_{eff} \cos\theta_C = K\lambda/\langle d \rangle + 2\varepsilon \sin\theta_C$, where K is Scherrer constant (0.89), ε is the lattice strain and $\beta_{eff}^2 = \beta^2 - \beta_0^2$. In this case, the $2\theta_C$ and β values were calculated by fitting the XRD peak profile to Voigt shape and β_0 is the full width at half maximum of standard Silicon powder. Finally, seven prominent XRD peaks were used for the $\beta_{eff} \cos\theta_C$ vs. $2\sin\theta_C$ plot. The linear extrapolation of this plot to $\beta_{eff} \cos\theta_C$ axis gives $K\lambda/\langle d \rangle$ (and hence, grain size $\langle d \rangle$) and the slope gives the lattice strain (ε). The calculated values of grain size and lattice strain are shown in Table 1. It is observed that the grain size calculated using Willimson-Hall plot is larger than that obtained from simple Debye-Scherrer formula, although the nature of the variation of grain size with milling time and annealing time is identical in both the cases. It is also observed that lattice strain of the alloyed compound increases with milling time and thermal annealing at 700°C reduces the lattice strain of the alloy. Similar effects were observed in other mechanical alloyed compound [20]. The lattice parameter of the samples (shown in Table 1) was calculated by matching the XRD peaks into rhombohedral structure with R3C space group. The lattice parameters (*a* and *c*) and cell volume of the alloyed compound were increasing with the milling time. But, the lattice parameters of the annealed samples showed decreasing values with the increase of annealing time at 700°C. The finite amount of mechanical milling induced lattice strain and its release by thermal annealing may have some effect on the variation of lattice parameters of the samples. However, the understanding of the variation of cell parameters is more appropriate from the fact that lattice parameters of bulk Cr_2O_3 sample (*a* = 4.9510 , *c* = 13.5996, cell volume = 288.69^3) is smaller than that for bulk α-Fe_2O_3 sample (*a* = 5.0386, *c* = 13.7498, cell volume = 302.3^3). The calculated lattice parameters for both bulk samples are consistent with literature values [4,5]. The continuous increase of lattice parameters and cell volume with milling time indicates the kinetic diffusion of larger size (0.67) Fe^{3+} ions into the boundary of smaller size (0.65) Cr^{3+} ions [2,4,21]. On the other hand, the decrease of cell parameters with the increase of annealing time indicated that the alloying process is, still, continued to attain the crystal structure of Cr_2O_3 dominated phase, because atomic ratio of Cr and Fe is 7:3. Here, it is pointed out that thermal heating plays a major role for obtaining the Cr_2O_3 dominated phase. It is believed that the variation of cell parameters is not significantly affected by the nano-sized grains in comparison with the undergoing change during alloying and annealing process. The cell parameters and grain size of the MA0 sample were not calculated, as the pattern is not due to single phase XRD spectrum.

Table 1: Grain size (<d>), lattice strain (ε) based on Willimson-Hall method and cell parameters of the samples are calculated using XRD data.

Sample	Grain size (nm)	Latice-strain	Lattice parameter a()	Lattice parameter c()	Volume ()^3
α-Fe$_2$O$_3$	--	--	5.0386 ± 0.0014	13.7498 ± 0.0002	302.30 ± 0.0840
MA0	--	--	--	--	--
MA24	63	0.4817 ± 0.0756	4.9521 ± 0.0021	13.6063 ± 0.0004	288.96 ± 0.1221
MA48	46	0.5121 ± 0.0365	4.9535 ± 0.0016	13.6041 ± 0.0002	289.08 ± 0.0923
MA84	35	0.5771 ± 0.0604	4.9546 ± 0.0013	13.6082 ± 0.0003	289.29 ± 0.0781
SN1	55	0.4495 ± 0.0416	4.9526 ± 0.0019	13.6142 ± 0.0002	289.19 ± 0.1090
SN3	74	0.3709 ± 0.0118	4.9520 ± 0.0018	13.6084 ± 0.0002	288.99 ± 0.1099
SN17	86	0.3202 ± 0.0121	4.9512 ± 0.0012	13.6070 ± 0.0002	288.87 ± 0.0997
Cr$_2$O$_3$	--	--	4.9510 ± 0.0011	13.5996 ± 0.0001	288.69 ± 0.0667

The parameters are not calculated for MA0 sample, due to the coexistence of two XRD patterns.

The surface morphology (SEM picture) and chemical composition (EDX spectrum) can be studied for selected (MA0, MA48, MA84 and SN17) samples. The selected zone (~80 μm × 80 μm) of the samples, along with SEM picture and EDX spectrum, are shown in Fig. 3. The SEM picture of MA0 sample (Fig. 3a) suggests the heterogeneous mixed character of α-Fe$_2$O$_3$ and Cr$_2$O$_3$ particles. The mechanical alloying between α-Fe$_2$O$_3$ and Cr$_2$O$_3$ particles can be understood

from the SEM picture of MA84 sample (Fig. 3b), where nanoparticles are distributed with a little bit agglomeration. A better uniformity in the particle size distribution is observed from the SEM picture (Fig. 3c) of thermal activated (SN17) sample. The elemental composition of the samples is determined from the point and shoots microanalysis at 10 selected points over a selected zone. The elements are found to be Cr, Fe and O. The atomic percentage of the elements is estimated from the EDX spectrum of the samples and Fig. 3d represents the spectrum for MA84 sample. The composition of Cr and Fe varies from 0.33 to 1.34 and 1.64 to 0.57, respectively, with respect to O composition 3 in MA0 sample. This suggests a random mixing of Fe$_2$O$_3$ and Cr$_2$O$_3$ oxides (i.e., an inhomogeneous distribution of elements) in MA0 sample. We obtained the atomic % of Fe (12.12), Cr (27.88) and O (60) (i.e., elemental composition Cr$_{1.38}$Fe$_{0.6}$O$_{2.97}$) for MA84 sample; atomic % of Fe (11.96), Cr (27.06), O (60.17) (i.e., elemental composition Cr$_{1.36}$Fe$_{0.6}$O$_{3.01}$) for SN17 sample. Therefore, elemental composition of the alloyed as well as annealed samples is close to the expected composition (Cr$_{1.4}$Fe$_{0.6}$O$_3$). The distribution of Cr, Fe and O atoms in the alloyed samples are cross checked from elemental mapping over a selected zone, as shown in Fig. 4 for MA48 sample. The mapping (Fig. 4c–e) suggests a uniform distribution of Cr, Fe, O atoms over the zone. The particle size (~500 nm) of MA48 sample estimated from the SEM picture (Fig. 4b) is much larger than that obtained from XRD data (~46 nm using
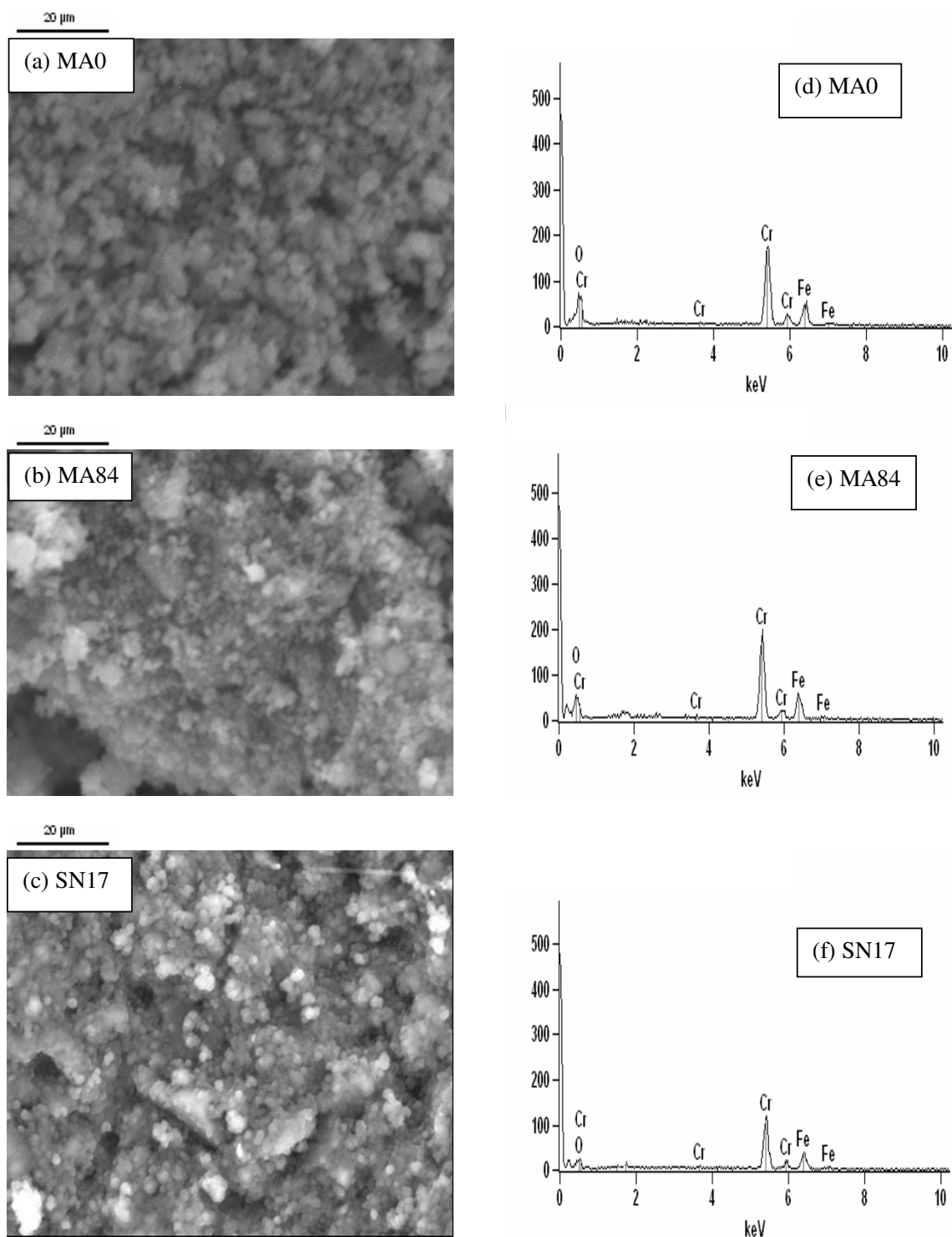
Figure 3
SEM picture of selected samples MA0 (a), MA84 (b), SN17 (c) and EDX spectrum of samples MA0 (d), MA84 (e), SN17 (f).
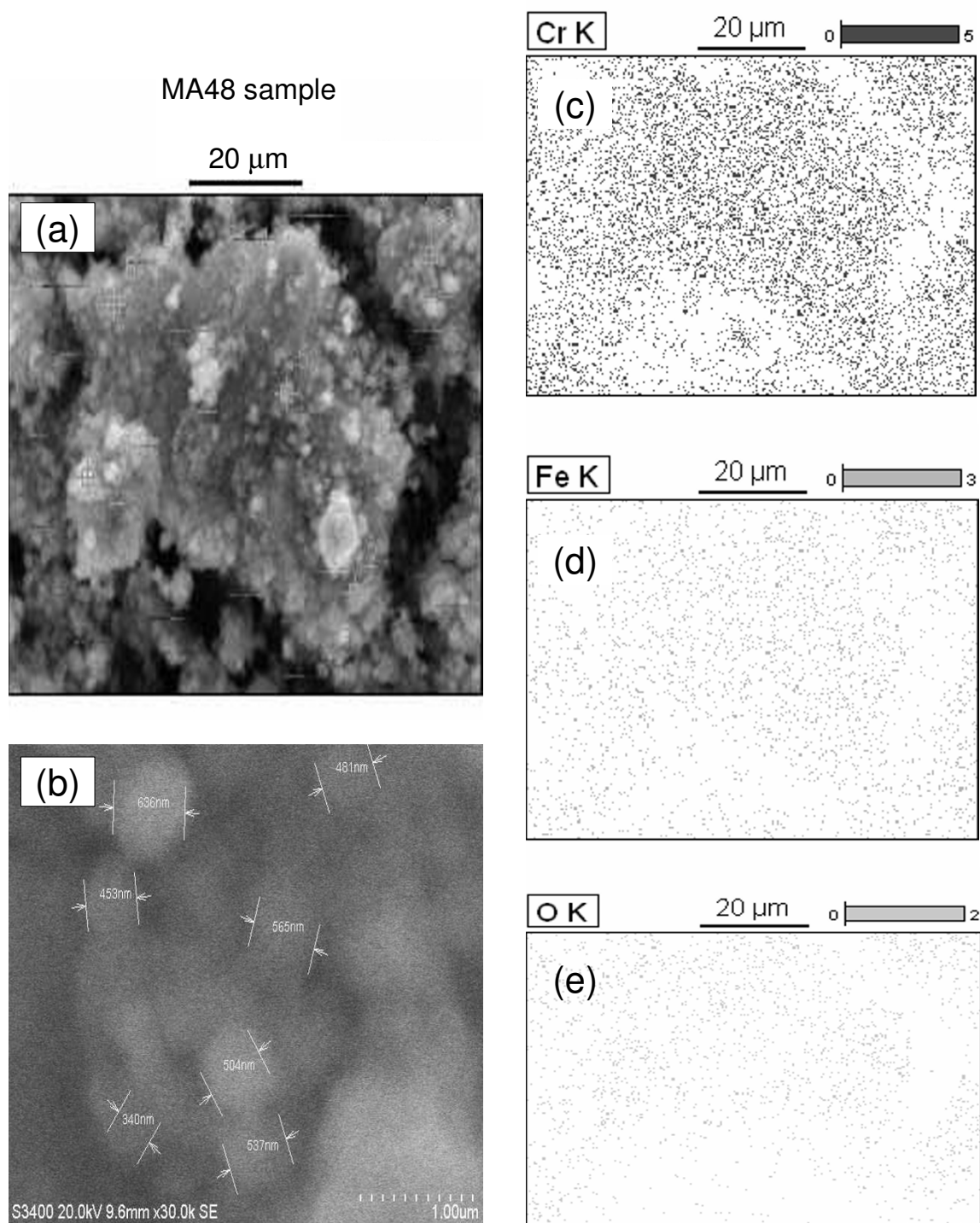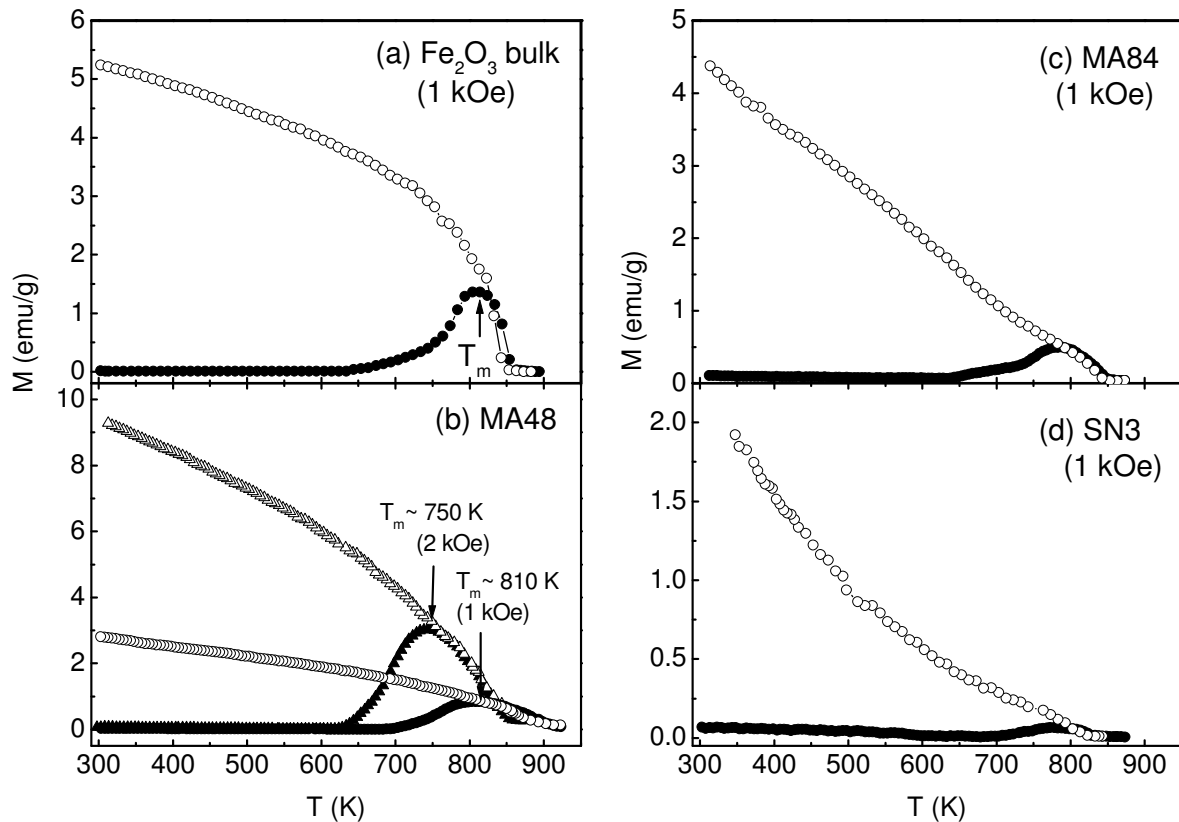
Figure 4
(Colour online) Selected zone (a) is used to estimate the particle size (b) and mapping of Cr (c), Fe (d) and O (e) atoms in MA48 sample.

Williamson-Hall method). This means the SEM picture indicates the size of polycrystalline particles. Achieving some basic knowledge of the structural properties (i.e., size, shape, composition, and crystal structure) of the samples, attempt has made below to understand the magnetic properties of the samples.

3.2. Magnetic properties

Fig. 5 shows the temperature dependence of ZFC and FC magnetization curve of different samples. The zero field cooled magnetization (MZFC), measured at 1 kOe field, does not change sig

nificantly (plateau like behaviour) in the temperature range 300 K to 600 K. The MZFC increases rapidly above 650 K to show a peak at about $T_m \sim 810$ K and then, MZFC rapidly decreases to indicate weak temperature dependence above 870 K. On the other hand, field cooled magnetization (MFC) at 1 kOe separates out from MZFC (i.e., onset of magnetic irreversibility) below the irreversibility temperature $T_{irr} \sim 860$ K. The separation between MFC and MZFC continued to

Figure 5
Temperature dependence of zero field cooled (solid symbol) and field cooled (open symbol) magnetization at 1 kOe for the selected (Fe$_2$O$_3$ bulk, MA48, MA84, SN3) samples. T_m represents the peak temperature of zero field cooled magnetization maximum. Magnetization data at 2 kOe are also shown to show the field dependence of T_m.

increase with the decrease of temperature down to 300 K. The above features of MZFC and MFC are seen in the bulk α-Fe_2O_3 sample, as well as in the alloyed $Cr_{1.4}Fe_{0.6}O_3$ samples, except some typical changes in the shape of the curves. The continuous increase of MFC with down curvature is observed in both bulk α-Fe_2O_3 and alloyed samples (e.g., MA48 and MA84). Interestingly, the shape of MFC curves of the annealed samples (e.g., SN3) has transformed into up curvature as an effect of thermal heating. The magnetization of bulk α-Fe_2O_3 sample decreases in the alloyed samples. The decrease is, further, accelerated by subsequent annealing of MA84 sample at 700°C. The decrease of magnetization is also reflected in the suppression of peak magnetization at T_m, when the sample changes from bulk α-Fe_2O_3 to SN17. We noted that the position of MZFC maximum at T_m is highly sensitive to the magnitude of measurement field. This is confirmed from the decrease of $T_m \sim 810$ K (at 1 kOe) to 750 K (at 2 kOe) in MA48 sample (Fig. 4b). The paramagnetic to canted ferromagnetic ordering temperature $T_N \sim 950$ K of bulk α-Fe_2O_3 (hematite) sample [reported in Ref. [4]] is higher than $T_m \sim 810$ K at 1 kOe (in the present work). The field dependence of T_m (~940 K at 100 Oe and ~845 K at 200 Oe) has already reported in bulk α-Fe_2O_3 (hematite) sample [22,23]. The present work showed that T_{irr} (~860 K) is higher than T_m (~810 K) and T_m decreases with the increase of measurement field. Based on these facts, we suggest that T_m does not represent a paramagnetic to canted ferromagnetic ordering temperature of the samples. Rather, T_m can be attributed as the temperature below which magnetic domains are blocked along the local anisotropy axes, where anisotropy energy might be higher than the measurement field [24-26]. The interesting point is that magnetic phase of α-Fe_2O_3 is, still, dominating in the alloyed compound, of course with diminished magnitude with milling time. This can be attributed to the presence of larger atomic moment of Fe^{3+} ions (~5 μ_B) in comparison with Cr^{3+} ions (~3 μ_B). The effect of α-Fe_2O_3 phase is becoming weak in the annealed samples, as seen from the weak magnetic irreversibility and upward curvature in the MFC curve of SN3 sample. The results clearly showed that Cr_2O_3 dominated typical antiferromagnetic phase in the alloyed compound is yet to achieve at 700°C. The diffusion of Fe atoms into the Cr lattices either still continues, although the XRD data indicated the stabilization of alloyed $Cr_{1.4}Fe_{0.6}O_3$ close to the pattern of Cr_2O_3 sample. The appearance of a different kind of magnetic behaviour in the annealed samples may also be attributed to a modulated magnetic ordering at the interface of nano-sized grains.

The existence of possible modulated magnetic phase in the samples is investigated from the field dependence of dc magnetization. The magnetization (M) with the variation of field (H) at room temperature is shown in Fig 6. The M(H) data of bulk Fe_2O_3 and Cr_2O_3 are shown in Fig. 6a to compare the magnetic change in alloyed compound. Bulk Cr_2O_3 sample does not show any noticeable hysteresis loop, whereas Fe_2O_3 sample has shown a well defined loop. The mixture of Fe_2O_3 and Cr_2O_3, i.e., MA0 sample (Fig. 6b), shows a clear loop, but the magnitude of loop of MA0 sample is less in comparison with Fe_2O_3. This is due to the effect of Cr_2O_3 coexisting with Fe_2O_3. As the alloying process continued by increasing the milling time, the loop area gradually
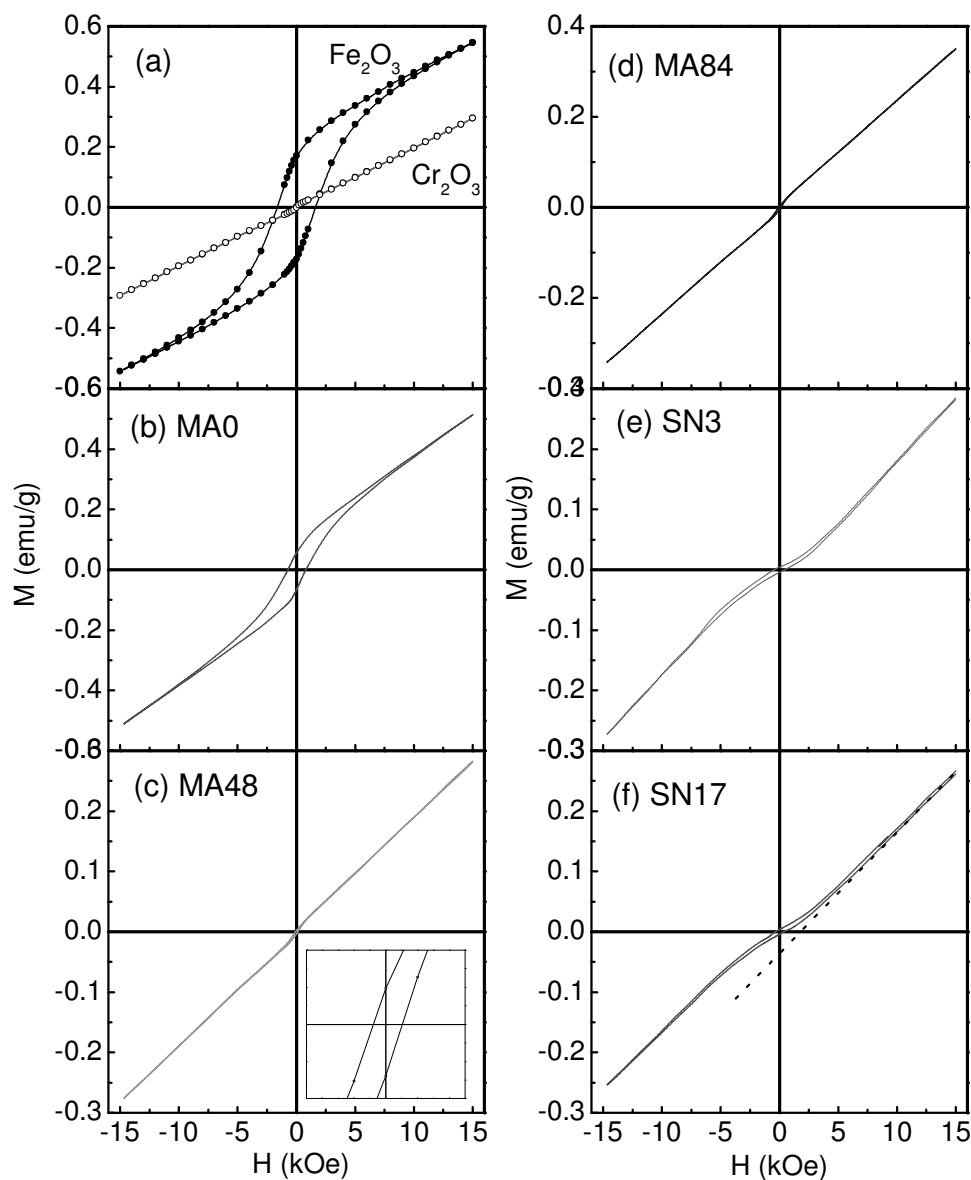
Figure 6
Variation of magnetization (M) with applied field (H) for different alloyed samples, along with bulk Fe$_2$O$_3$ and Cr$_2$O$_3$ samples. The existence of a small hysteresis loop for MA48 sample is shown in the inset of (c).

decreases, but noticeable, as shown for MA48 sample in the inset of Fig. 6c. It is interesting to note that the nature of M(H) curves of annealed samples (Fig. 6e–f) drastically differ in comparison with the mechanical alloyed samples. The extrapolation of high field M (positive H side) data (shown by dotted line in Fig. 6f) intersects the M axis to negative value and the negative magnetization confirmed the field induced magnetic behaviour in the annealed samples. We would like to mention that neither bulk Fe$_2$O$_3$ nor bulk Cr$_2$O$_3$ sample exhibited such induced magnetization. Recently, similar field induced magnetization has been observed in the Cr$_2$O$_3$ nanopar-

ticles [27], originating from the competitive spin ordering at the core-shell interface [28]. Viewing the absence of such field induced magnetic ordering in mechanical alloyed (with out heat treatment) samples, although grain size is in nanometer range, we believe that the field induced mag

netic behaviour in our annealed samples is not solely due to particle size effect, but can be attributed to a modulated magnetic ordering due to diffusion of two different magnetic elements [29]. The induced magnetic behaviour in annealed samples is also reflected in the field dependence of differential magnetization (dM/dH) curves (Fig. 7). The differential susceptibility (dM/dH) increases to exhibit a maximum for mechanical alloyed samples when the applied field approaches to zero value, whereas dM/dH exhibits a minimum near to the zero field value for the annealed samples. The observation of induced magnetism confirms an experimental evidence of modulated spin structure in this compound, which was suggested from Neutron diffrac

tion study [8]. To get the insight of modulated magnetic ordering, we analyze the M(H) data in terms of a general power series of H, i.e., the combination of liner and non-linear components in the equation

$$M(H) = \chi_1 H + \chi_2 H^2 + \chi_3 H^3 + (\text{rest of the terms}) \qquad (1)$$

In the above equation, we have assumed that magnetic susceptibility is not a scalar quantity, rather a tensor with directional property in the material. The coefficients χ_1 and χ_3 are assumed to be symmetric with field (H), where as χ_2 is antisymmetry to preserve the vector nature of magnetization (M). The validity of equation (1) is tested from Fig. 8. The M vs. H^2 data (in Fig. 8a)

indicate that magnetization of all the samples are symmetric about the H^2 axis, irrespective of alloyed or annealed samples, and the change of magnetic direction is taken care by χ_2, i.e., $\chi_2(-H) = -\chi_2(H)$. It is really interesting to note that M vs. H^3 plot (Fig. 8b) represents a ferromagnetic like appearance, irrespective of the samples and confirms the symmetric nature of χ_3, where the change of magnetization direction is taken care by H. The investigation of non-linear components (specially the second-harmonic generation) in antiferromagnetic material may be one of the important technological aspects of the present material.

Now, look at the magnetic parameters. The remanent magnetization (M_R) and coercive field (H_C) of the samples were calculated using M(H) data. The variation of M_R and H_C of the alloyed compound with milling time and annealing time is shown in Fig. 9. We noted that both H_C (~1620 Oe) and M_R (~172 memu/g) of α-Fe_2O_3 sample are reduced by nearly 2.5 times in MA0 sample (H_C ~ 700 Oe and M_R ~ 66.3 memu/g), although Cr_2O_3 is not showing any hysteresis loop. This feature suggests that properties of magnetic particles, irrespective of bulk (present
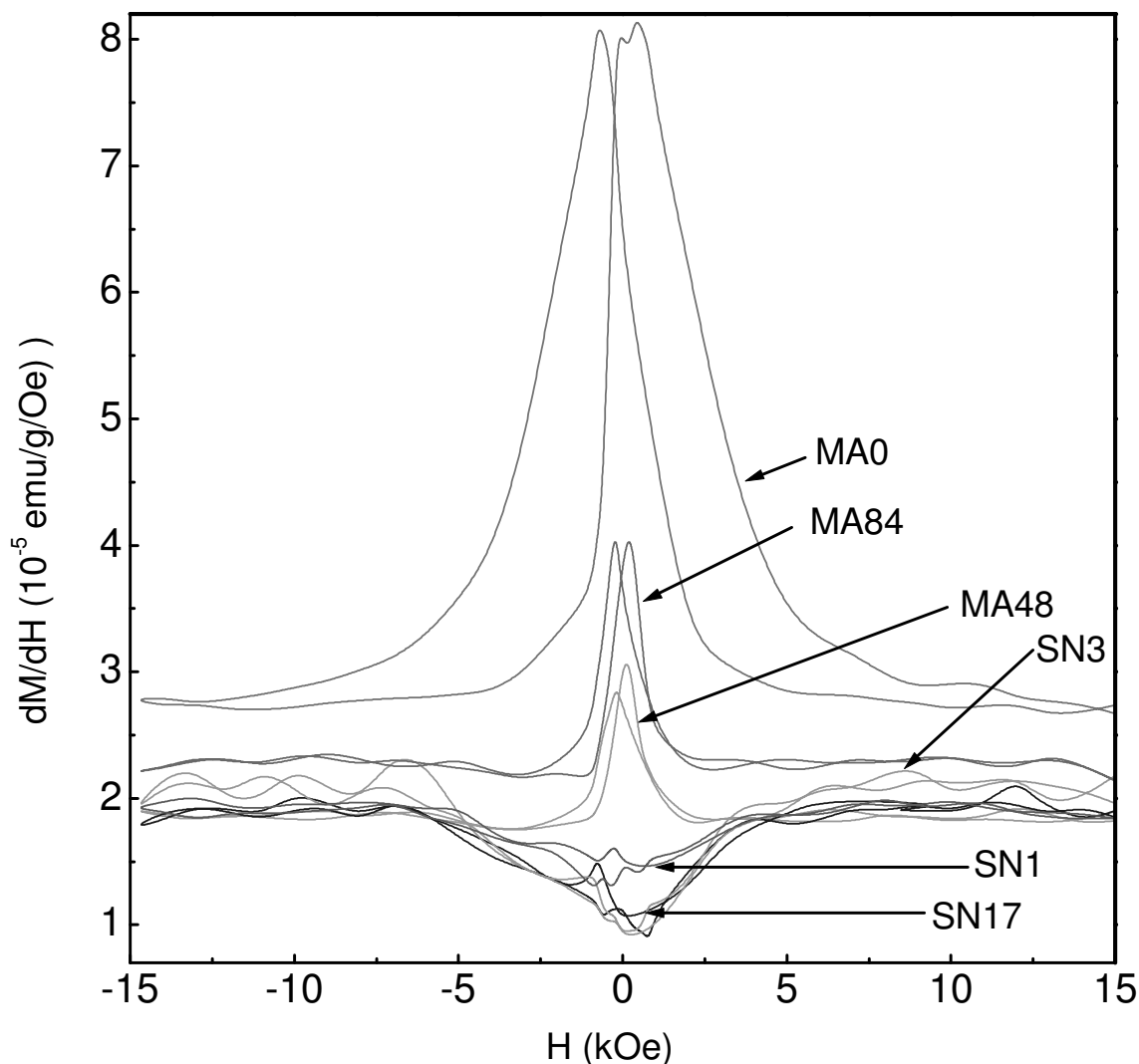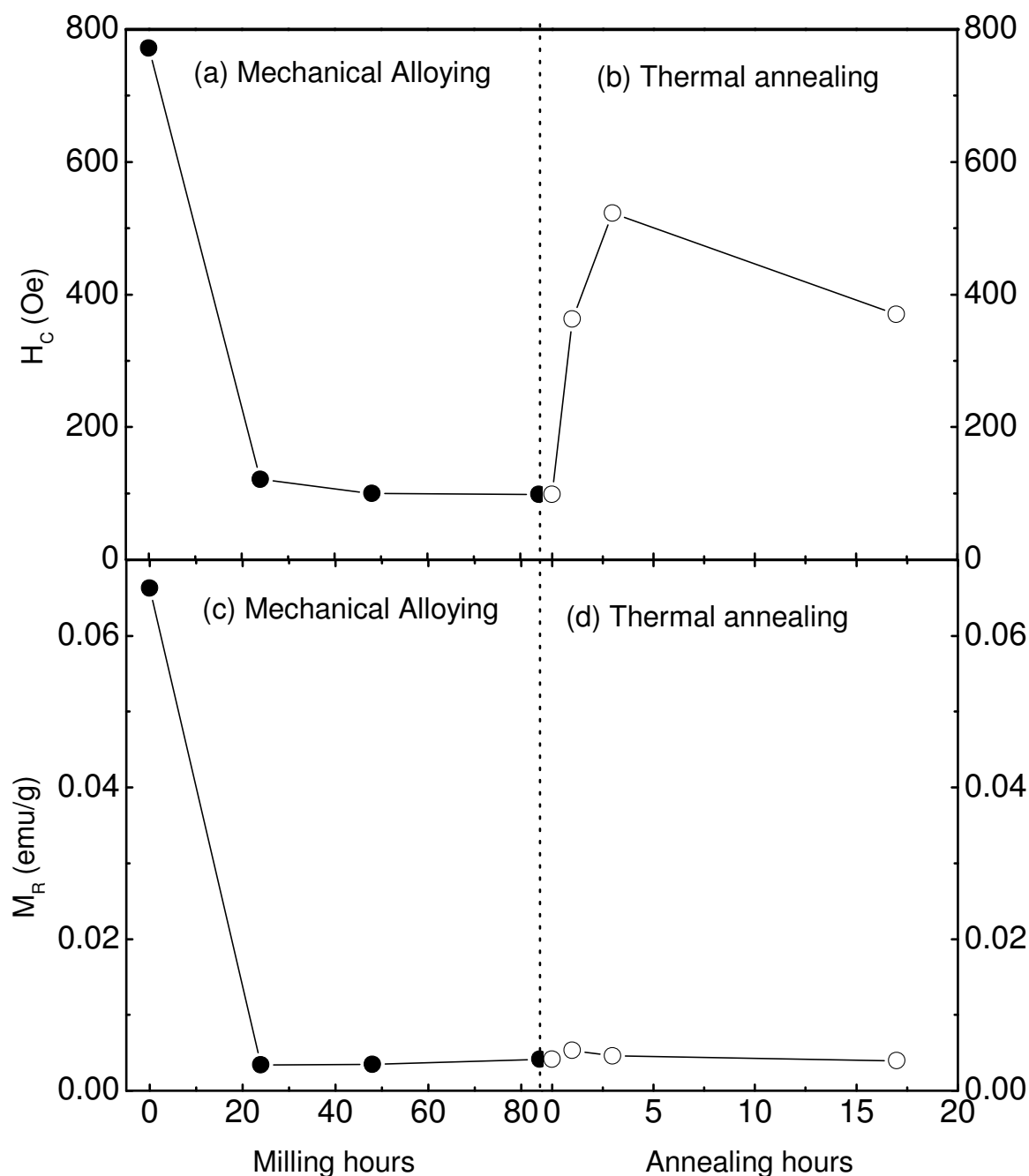
Figure 7
(Colour online) The field dependence of differential susceptibility (dM/dH) is shown for selected (MA0, MA48, MA84, SN1, SN3, SN17) samples.

work) or nanosize (reported work [30]), are strongly influenced by the surrounding matrix. The H_C of MA0 sample is continued to decrease with milling time (e.g., $H_C \sim 120$ Oe for MA24). On the other hand, H_C has shown a significant increase by annealing MA84 sample at 700°C up to 3 hours, followed by a slight decrease at 17 hours annealed sample (SN17). The M_R of MA0 sample also decreases to attain an almost constant value ~3.4 memu/g for MA24 and MA48 samples, followed by a slow increase (~4.4 memu/g) for MA84 sample and continued for (~5.3 memu/g) SN1 sample. The M_R value, again, starts to decrease at higher annealing time, e.g. ~3.9 memu/g for SN17 sample. The decrease of both remanent magnetization and coercivity at higher annealing time indicates that the alloyed compound is approaching to the magnetic state dominated by non-hysteretic Cr_2O_3 sample or a different kind of magnetic ordering that is already indicated
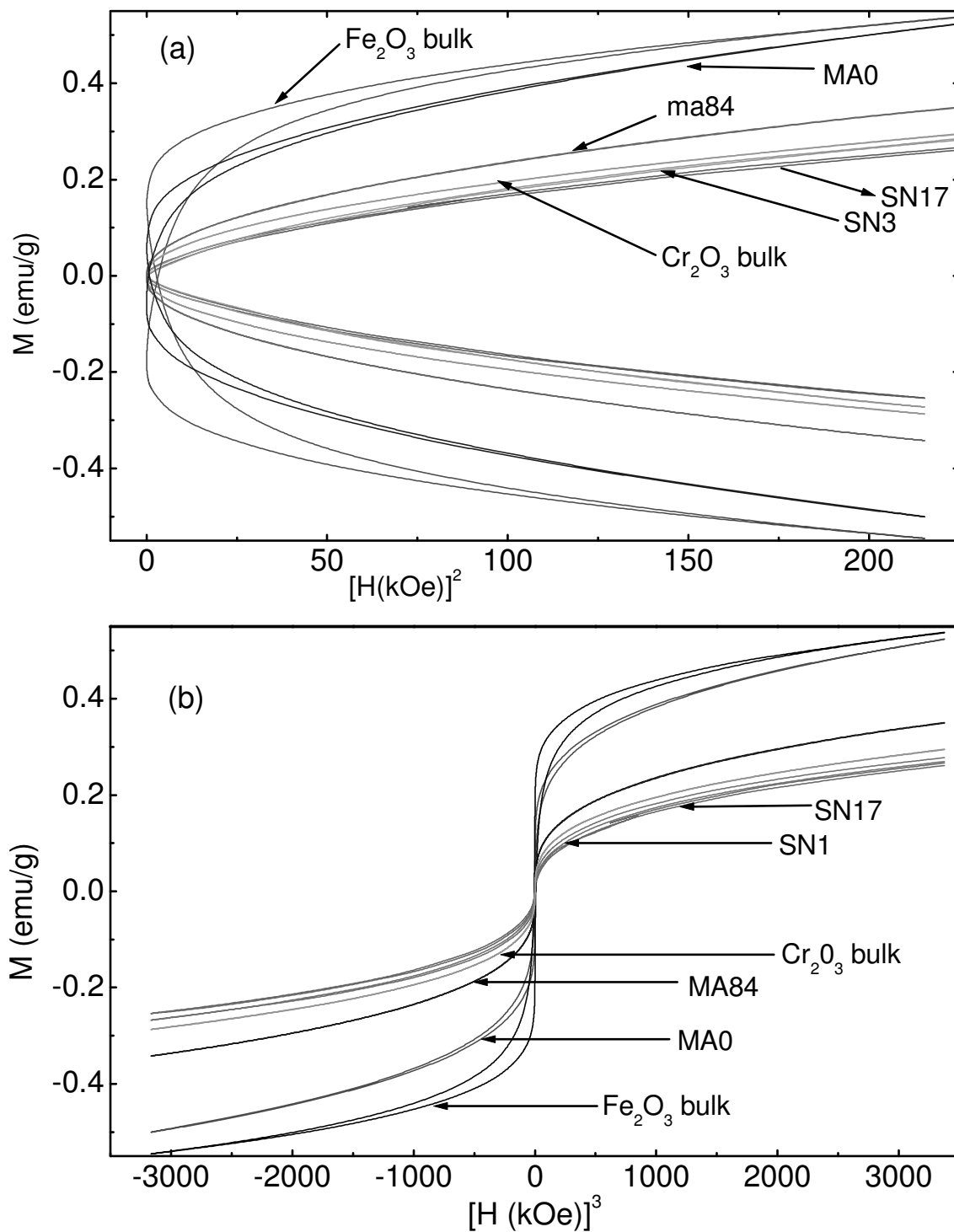
Figure 8
(Colour online) (a) M vs. H^2 plot and (b) M vs. H^3 plot for selected samples.

Figure 9
The variation of coercivity (H$_C$) and remanent magnetization (M$_R$), calculated from hysteresis loop, are shown with the variation of milling time and annealing time.

earlier. The fact is that mechanical alloying has introduced a certain amount of lattice strain (and defects) in the material. However, we did not find the increase of coercivity with increasing milling time (and associated increasing strain), rather the coercivity decreases. Hence, the effect of strain and associated defects is minor on the magnetic properties of the present alloyed compound and such effect can be included in the combined contribution of grain boundary spins.

4. Conclusion

The magnetic properties of mechanical alloyed $Cr_{1.4}Fe_{0.6}O_3$ compound strongly depends on the structural change associated with the variation of milling time and annealing temperature. The variation of cell parameters is attributed to the effect of diffusion of Fe^{3+} ions into the boundary of Cr^{3+} ions. The structural analysis, using XRD and SEM with EDX spectrum, may suggest the completion of alloy formation during milling process, but the magnetic behaviour confirmed that the alloying process is, still, continued at $700\,^\circ C$ to approach the structure dominated by Cr_2O_3 phase. Experimental results suggested that magnetic ordering of mechanical alloyed $Cr_{1.4}Fe_{0.6}O_3$ compound, annealed at $700\,^\circ C$, belongs to neither a canted ferromagnetic ordering of α-Fe_2O_3 nor a typical antiferromagnetic ordering of Cr_2O_3. Rather, a field induced magnetic

order appeared in the annealed samples, which we attribute to the appearance of a modulated spin structure in the compound. This experimental work may instigate subsequent investigations on the non-linear magneto-opto-electronic properties of similar materials.

References

1. Cox PA: **Transition Metal Oxides: An Introduction to Their Electronic Structure and Properties (Clarendon, Oxford, 1992).** .

2. Jaffe JE, Dupuis M, Gutowski M: *Phys Rev B* 2004, **69:**205106.

3. Levistein HJ, Robbins M, Capio C: *Mater Res Bull* 1972, **7:**27.

4. Yin-Yuan Li: *Phys Rev* 1956, **101:**1450.

5. McCarty KF, Boehme DR: *Journal of Solid State Chemistry* 1989, **79:**19.

6. Music S, Lenglet M, Popovic S, Hannoyer B, Czako-Nagy I, Ristc M, *et al.*: *J Mater Sci* 1996, **31:**4067.

7. Osmond WP: *Proc Phys Soc* 1962, **79:**394.

8. Cox DE, Takei WJ, Shirane G: *J Phys Chem Solids* 1963, **24:**405.

9. Dzyaloshinskii IE: *Zh Eksp Teor Fiz* 1959, **37:**881. [Sov. Phys. JETP **10**, 628 (1960)]

10. Astrov DN: *Zh Eksp Teor Fiz* 1960, **38:**984. [Sov. Phys. JETP **11**, 708 (1960)]

11. New D, Lee NK, Tan HS, Castner TG: *Phys Rev Lett* 1982, **48:**1208.

12. Schmid H: *Ferroelectrics* 1994, **161:**1.

13. Hill NA: *J Phys Chem B* 2000, **104:**6694.

14. Di Matteo S, Natoli CR: *Phys Rev B* 2002, **66:**212413.

15. Merchant P, Collins R, Kershaw R, Dwight K, Wold AJ: *Solid State Chemistry* 1979, **27:**307.

16. Bhattarcharya AK, Hartridge A, Mallick KK, Majumdar CK, Das D, Chintalapudi SN: *Journal of Material Science* 1997, **32:**557.

17. Manjanna J, Venkateswaran G: *The Canadian Journal of Chem Eng* 2002, **80:**882.

18. Chicinas IJ: *Optoelectronics and Advanced Materials* 2006, **8:**439.

19. Williamson GK, Hall WH: *Acta Metall* 1953, **1:**22.

20. Hamzaoui R, Guessasma S, ElKedim OJ: *Alloys and Comp* 2008, **462:**29.

21. Chambers SA, Droubay T: *Phys Rev B* 2001, **64:**075410.

22. Zysler RD, Vasquez-Mansilla M, Arciprete C, Dimitrijewits M, Rodriguez-Sierra D, Saragovi C: *J Magn Magn Mater* 2001, **224:**39.

23. Vasquez Mansilla M, Zyslera R, Fiorani D, Suber L: *Physica B* 2002, **320:**206.

24. Bhowmik RN, Ranganathan R, Nagarajan R: *J Magn Magn Mater* 2006, **299:**327.

25. Aharoni A, Frei EH, Schieber M: *Phys Rev* 1962, **127:**439.

26. Lin ST: *Phys Rev* 1959, **116:**1447.

27. Tobia D, Winkler E, Zysler RD, Granada M, Troiani HE: *Phys Rev B* 2008, **78:**104412.

28. Bhowmik RN, Nagarajan R, Ranganathan R: *Phys Rev B* 2004, **69:**054430.

29. Abe R, Tsunoda Y, Nishi M, Kakurai K: *J Phys Condens Mater* 1998, **10:**L79.

30. Frandsen C, Morup S: *J Magn Magn Mater* 2003, **266:**36.